Negative transients in central-loop time-domain electromagnetic data: Induced polarization or 3D coupling effect?

Dikun Yang[1], Ming Cheng[1] and Qiang Luo[2]
[1] Southern University of Science and Technology (SUSTech)
[2] Guangdong Provincial Geophysical Prospecting Team

SUMMARY

Negative transient data in time-domain electromagnetic (TEM) are often explained by the induced polarization (IP) effect. However, a field example from a mineral exploration site in China proves that the 3D coupling effect, as a result of the strong literal variation in conductivity, can be a more appealing explanation. This article presents an interesting TEM dataset that confused geophysicists who were used to the conceptual model of 1D layered earth. Using the advanced fast 3D modeling tools accelerated by the survey decomposition method and decentralized massive parallel computing, we can quickly establish some representative block models that help us understand and verify the mechanism of negative transient TEM data. The forward modeling exercises also generates a good candidate of the initial model for the subsequent inversion process, as the regular uniform subsurface models may lead to a non-convergence due to local minima. The outcome of our research is a robust workflow for 3D inversion in practice: fast forward simulation of ballpark models to search for an initial model sufficiently close to the truth, then warm-start the 3D inversion to fine-tune the small-scale structures.

Keywords: time-domain electromagnetic, three-dimensional, inversion, negative transients, induced polarization

INTRODUCTION

The central-loop configuration of time-domain (transient) electromagnetic (TEM) places the receiver coil at the middle of the transmitter loop. Such a configuration, as well as the ones with a transmitter-receiver offset sufficiently small, has the advantage of a strong source-target-receiver coupling and the ability of being adopted for airborne and other mobile platforms (Maurya et al., 2023).

It also appears repeatedly in literatures that the central-loop configuration can be used to discriminate the induced polarization (IP) effect, which is indicative in mineralization, soil contamination and other applications. Theoretical studies have proven that only chargeable earth media characterized by the Cole-Cole model or alike can generate negative transient data for coincident loop systems (Weidelt, 1982). Recently, a number of works, particularly for the airborne TEM, have proposed different methods to extract valuable IP information from the negative data that were once discarded as uninterpretable data (e.g. Legault, 2015; Kang & Oldenburg, 2016; Maurya et al., 2022).

However, to use the inductive source central-loop TEM for IP, one has to assume that the source loop can be regarded as a magnetic dipole. For non-dipole loop sources, negative central-loop data may not necessarily be the IP effect. This article reports a real dataset with negative transients that were thought to be the IP effect but later numerically and geologically proven to be the 3D coupling effect.

In the following, we first describe the background of the site, the survey and the data; then some numerical tools were developed to enable people to efficiently explore the possibilities of 3D effects; eventually, we demonstrate how we used the tools to solve the puzzle, and to yield a conclusive model through a warm-started 3D inversion.

SURVEYS AND DATA

The field data were collected at a polymetallic mining site in Guangdong province, south China. The survey area is composed of two distinct geologic units, the Cambrian Gaotan Formation made of fine-grained quartz sandstone and the Cambrian Niujiaohe Formation composed of siltstone and metamorphic sandstone (Figure 1). Rock samples from the Gaotan Formation on the southeastern side of the area have measured resistivities from 8000 to 20000 Ω·m; the Niujiaohe Formation on the northwestern side is in the range from 46 to 200 Ω·m.

A survey line of receiver stations was planned from the distance 340 to 2160 m at a 10 m spacing. Six rectangular transmitter loops of 750 × 150 m were deployed to cover the entire line, so that the receiver stations are always in the central portion of the loop where the primary magnetic field is mostly vertical (Figure 1). At each station, the

dBz/dt data were measured at 28 time channels from 0.05262 to 24.291 ms with a step-off current waveform.

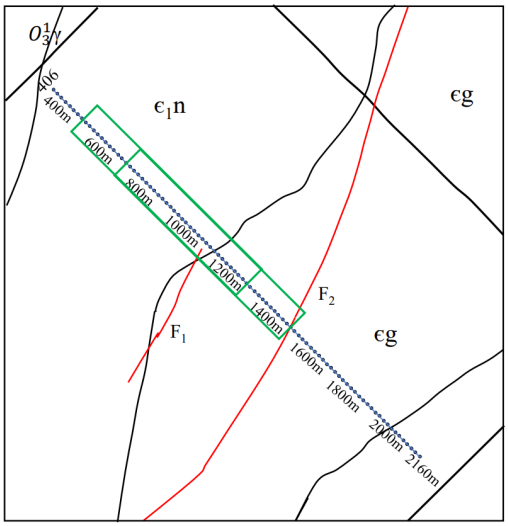

Figure 1: Geological map and the survey layout. The blue dots mark the receiver stations; two of the six rectangular transmitter loops are outlined by green.

The TEM decay patterns along the line is variable (Figure 2). Consistently normal and slow decays are observed at the stations smaller than 1000 m (Figure 3a); clear positive-negative sign flips are found at the stations around 1000 m (Figure 3b); the stations beyond 1100 m are characterized by rapid positive decays followed by noises (Figure 3c).

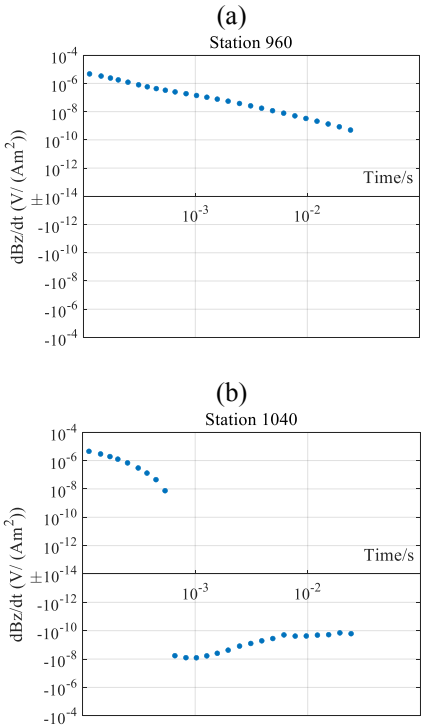

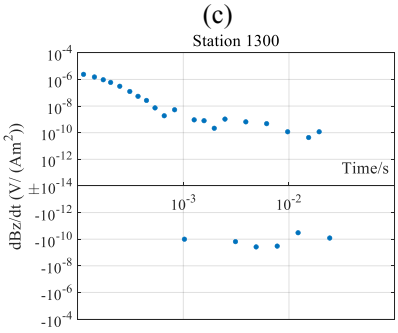

Figure 3: TEM decay data at select stations.

The 1D layered earth inversions were first performed (Figure 4). Some stations are missing on the cross section as the result of negative transient data and high noise. The negative transients around Station 1000 m are clear signals, and some practitioners proposed to interpret it using the Cole-Cole IP model. We did not think so. Most IP effects are found in a resistive background, where the induced currents can dissipate quickly, leaving alone the opposite discharging currents of the IP effect. It is unlikely IP-caused negative transients can be observed at the stations close to the conductive Niujiaohe Formation. Our hypothesis is that the rectangular source loop cannot be treated as a dipole source, and the 3D coupling between the large loop and the geologic structure is responsible for the sign flips in the central-loop data.

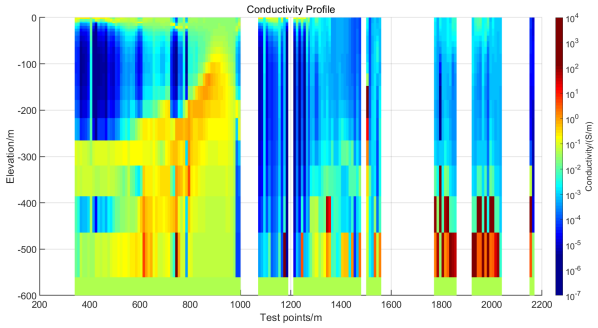

Figure 4: Stitched 1D inversion models.

SURVEY DECOMPOSITION METHOD

3D numerical simulation is necessary to verify our hypothesis. While rigorous 3D TEM modeling methods have been long established, practitioners often find it unpractical to use because of the long computing time compared with the 1D and plate modeling. In general, people manipulate models and expect to obtain the responses in seconds or minutes. To meet the need of timely trial-and-error forward modeling, we develop fast 3D modeling tools using the survey decomposition (SD) (Yang & Oldenburg, 2016).

In our implementation, the large source loop is treated as a combination of magnetic dipoles. Depending on the

time channel or the spatial scale of EM induction, the loop needs to be divided finely for the early times and coarsely for the late times. The resultant dipole source-receiver pairs are then efficiently modelled using local meshes customized for individual pairs (Figure 5). The time stepping for TEM is also decomposed to allow multiple time steps to be computed in parallel and at scale-adapted step sizes, so late times do not need to wait for the early times. Each decomposed subproblem is only for one datum and is solved on a local mesh only accommodating a dipole source and a receiver operating at a certain time channel.

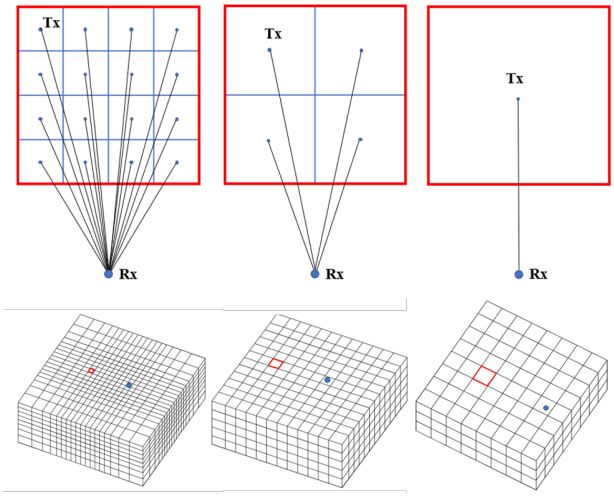

Figure 5: Decomposition of source loop and the local meshes for early (left), middle (middle), and late (right) time channels.

Our 3D TEM algorithm adopts the finite volume method on rectilinear meshes; the time stepping is based on the implicit backward Euler method; the linear system of equations is solved by the parallel direct solver MKL PARDISO; the code is written by C++. We present some metrics of an example TEM sounding (Table 1). The sounding consists of 25 time channels from 0.1 to 30 ms. The early times require finer decomposition of the loop and smaller time steps; for time channels later than 4.7 ms, the large loop can be effectively represented by a single magnetic dipole. The local meshes are relatively small at the order of dozens of thousands of cells. The computing time of each subproblem varies from 7 to 14 s. If the independent subproblems are solved on a cluster with sufficient nodes, the 3D modeling of this sounding can be finished in seconds.

The independency of subproblems after SD makes the method particularly suitable for massive parallelization. In another test with 2850 subproblems, SD shows a good linear scalability from 100 nodes (4000 cores) all the way up to 780 nodes (31200 cores) (Figure 6). Further speed-up can be expected on even larger clusters or cloud computing.

Table 1: Decomposed subproblems of one sounding.

Time Channels (s)	Time step (s)	Number of dipoles	Number of cells in local mesh	CPU time of a single subproblem(s)
1×10^{-4}	5.0×10^{-6}	16	28,800–29,760	7
1.208×10^{-4}	6.308×10^{-6}	16	28,800–29,760	7
1.499×10^{-4}	7.498×10^{-6}	16	28,800–30,720	7
2.005×10^{-4}	1.003×10^{-5}	9	29,760–31,620	8
2.499×10^{-4}	1.250×10^{-5}	9	29,760–31,620	8
3.001×10^{-4}	1.500×10^{-5}	9	30,720–32,640	8
3.813×10^{-4}	1.907×10^{-5}	9	30,720–32,674	8
4.805×10^{-4}	2.403×10^{-5}	4	32,640–34,782	9
7.108×10^{-4}	3.554×10^{-5}	4	33,660–35,836	9
9.475×10^{-4}	4.737×10^{-5}	4	34,680–35,836	9
1.204×10^{-3}	4.013×10^{-5}	4	35,700–36,890	9
1.699×10^{-3}	5.665×10^{-5}	4	36,720–37,800	10
2.149×10^{-3}	7.164×10^{-5}	4	36,750–37,800	10
2.599×10^{-3}	8.664×10^{-5}	4	36,750–37,800	10
3.498×10^{-3}	1.166×10^{-4}	4	36,750–37,944	10
4.749×10^{-3}	1.583×10^{-4}	1	39,060	11
5.498×10^{-3}	1.833×10^{-4}	1	40,320	11
5.999×10^{-3}	1.999×10^{-4}	1	40,460	11
8.249×10^{-3}	2.750×10^{-4}	1	41,616	11
1.075×10^{-3}	2.688×10^{-4}	1	44,064	12
1.325×10^{-2}	3.313×10^{-4}	1	45,928	12
1.600×10^{-2}	4.000×10^{-4}	1	46,656	13
2.175×10^{-2}	5.437×10^{-4}	1	47,952	13
2.550×10^{-2}	6.376×10^{-4}	1	49,248	14
3.000×10^{-2}	7.500×10^{-4}	1	51,840	14

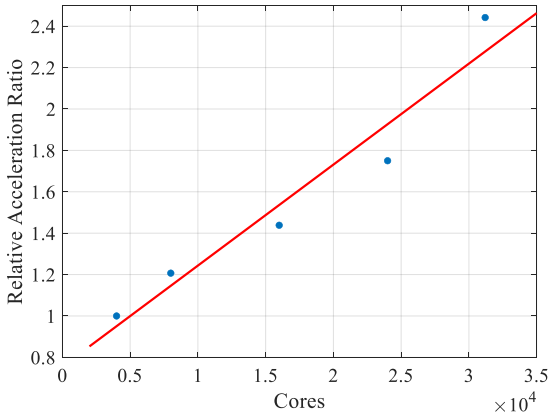

Figure 6: Acceleration in the environment of massive parallelization.

FORWARD SIMULATION

A number of block models are constructed to investigate the positive-negative transient data around Station 1000. Each forward modeling is decomposed to 1755 independent subproblems. The computing time of those subproblems on 50 cluster nodes is about 3.8 minutes, short enough for people to carry out trial-and-error simulations for hypothesis tests.

After some trials, we construct a contact model to reasonably reproduce the positive-negative transients observed in the field. The model consists of a resistive quarter-space of 10^{-4} S/m and a conductive quarter-space of 10^{-2} S/m; a very conductive block of 10^{2} S/m is embedded in the conductive side and is out-cropping. When the transmitter loop is placed across the contact

boundary (Figure 7a), the receivers off the conductor can observe sign-flipped transient data (Figure 7b).

We offer an intuitive explanation of such a phenomenon. At early times, the induced current is strong in both the conductive and the resistive sides, so the transients are positive. After a period of time, the induction on the resistive side disappears quickly, leaving only a horizontally circular eddy current on the conductive side. So, at late times, the receivers outside of the conductor measure the magnetic field generated by the slowly-decaying eddy current loop confined in the conductor.

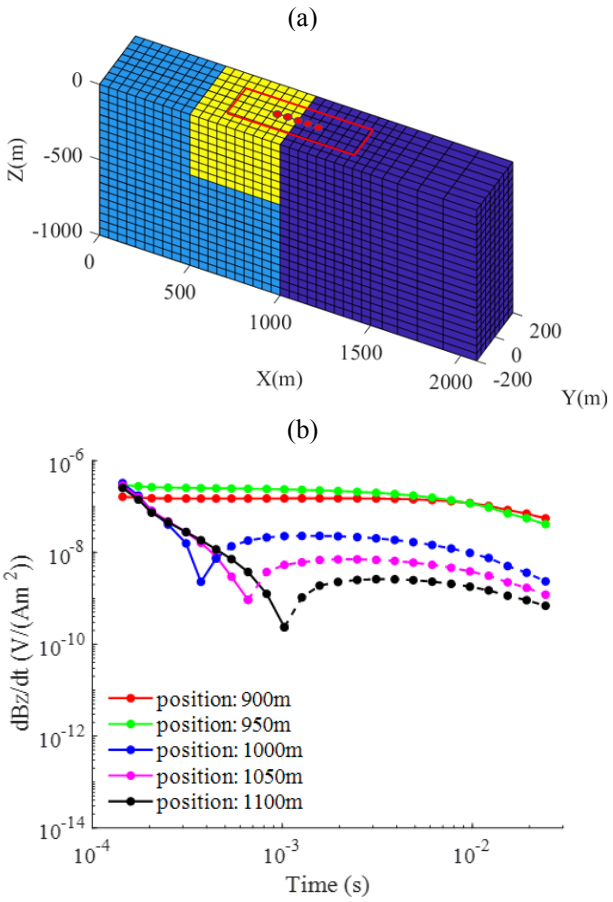

Figure 7: Forward simulation of conceptual models. (a) A contact and block model and the layout of source loop outlined by the red rectangle; (b) The simulated TEM data at the receiver locations marked by the red dots.

INVERSIONS

The TEM data from the transmitter loop that contains strong positive-negative transients (Figure 3b) are chosen for 3D inversion. The first attempt of 3D inversion is carried out with a starting model of a uniform subsurface. However, the inversion stalls in a local minimum after a few iterations with little improvement in the data misfit (Figure 8a). The recovered model does not represent anything geologically meaningful or tendency of moving towards reasonable models (Figure 8b). The reason is that it is impossible for the inversion to fit the negative data by knowingly generating strong lateral variations. Mathematically, the starting model is not sufficiently close to the true model, so the gradient-based model search may fail.

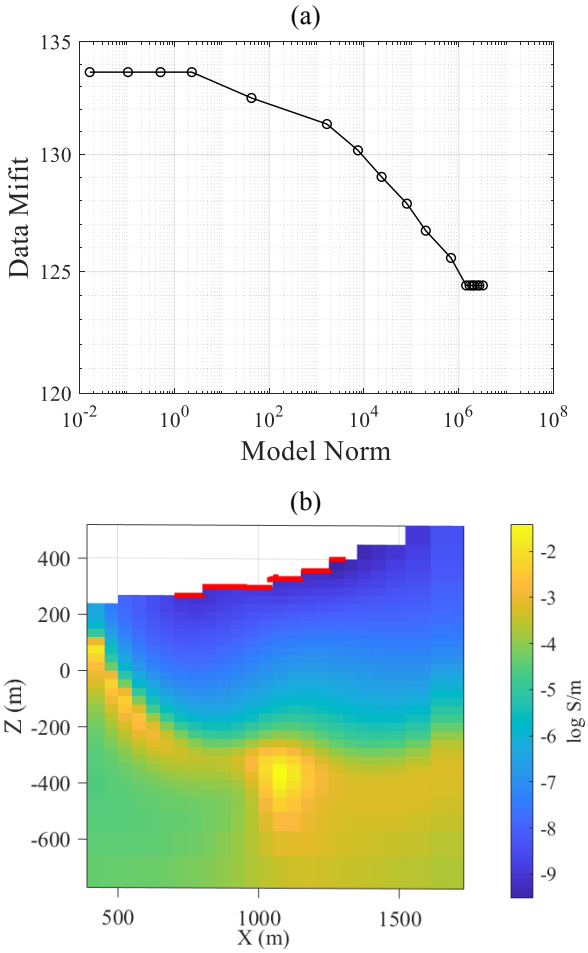

Figure 8: 3D inversion starting from a uniform subsurface. (a) Convergence curve of the data misfit; (b) Resultant conductivity model.

Next, the model from the forward simulation (Figure 7a) is used as the starting and reference model to "warm-start" the inversion. Although such a model contains some unrealistic conductivities and boundaries, it has the critical ability of generating positive-negative transients, a significant step in fitting the negative data. The subsequent inversion iterations can further polish the model in the L-2 smooth manner. The warm-start inversion is able to converge to a normalized misfit close to unity (Figure 9a). The positive-negative transient data are adequately fit (Figure 9b). The final inversion model resembles the ballpark structure in the starting model, but some small-scale features are fine-tuned by the inversion (Figure 9c). The final model confirms the contact between

the conductive Niujiaohe Formation and the resistive Gaotan Formation. The credibility of the model is also supported by an independently processed CSAMT 2D inversion model along the same survey line (Figure 9d).

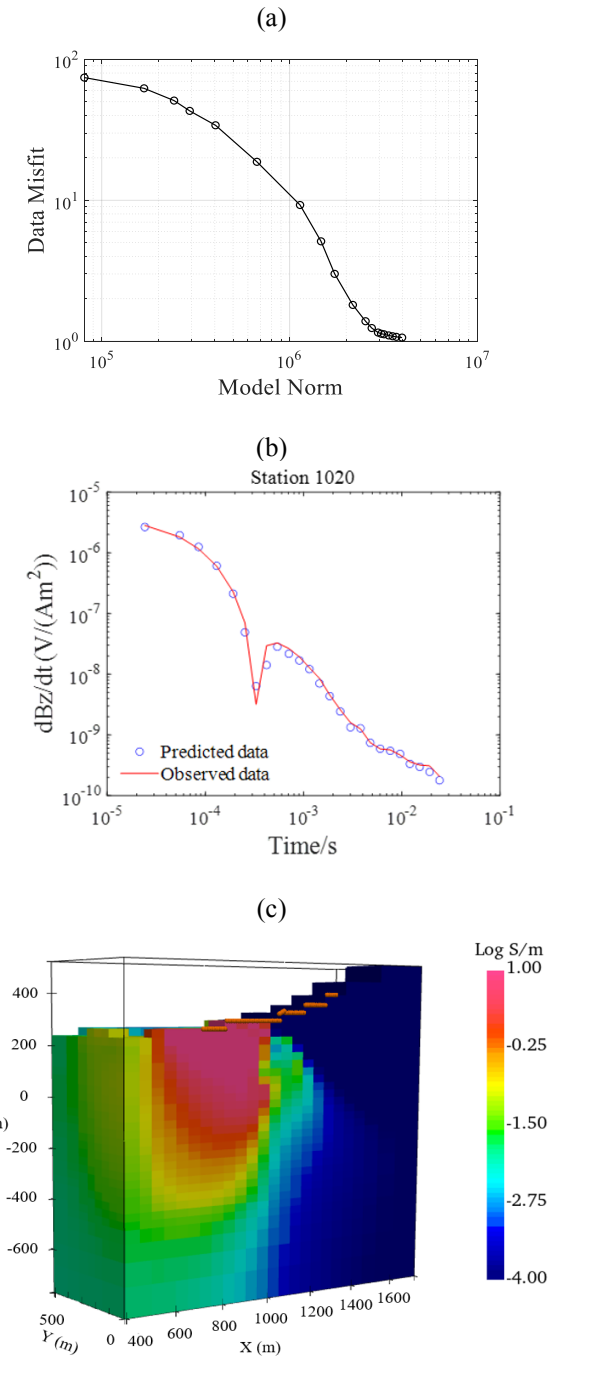

Figure 9: 3D warm-start inversion. (a) Convergence of the data misfit; (b) Fitting negative transient data; (c) Recovered 3D model; (d) CSAMT inversion result.

CONCLUSION

We presented an educational and inspiring case study that highlights the importance of 3D EM inversion and interpretation. The following can be learned.

Negative transient data in central-loop TEM are not necessarily the IP effect; the 3D coupling effect can also generate negative data if a large source loop encloses conductive and resistive terrains, and the in-loop receivers are off the conductive terrain.

The fast forward modeling powered by the survey decomposition is highly parallelizable and can respond to hypothetical model tests in seconds or minutes; the fast modeling tool is the key to quickly understand the measured data in practice.

We recommend to use the representative ballpark models from the forward exercise to warm-start the 3D inversion for a stable convergence and robust recovery of model.

ACKNOWLEDGEMENT

This work was funded by the Southern Marine Science and Engineering Guangdong Laboratory (Zhuhai) under the grant No. SML2021SP303.

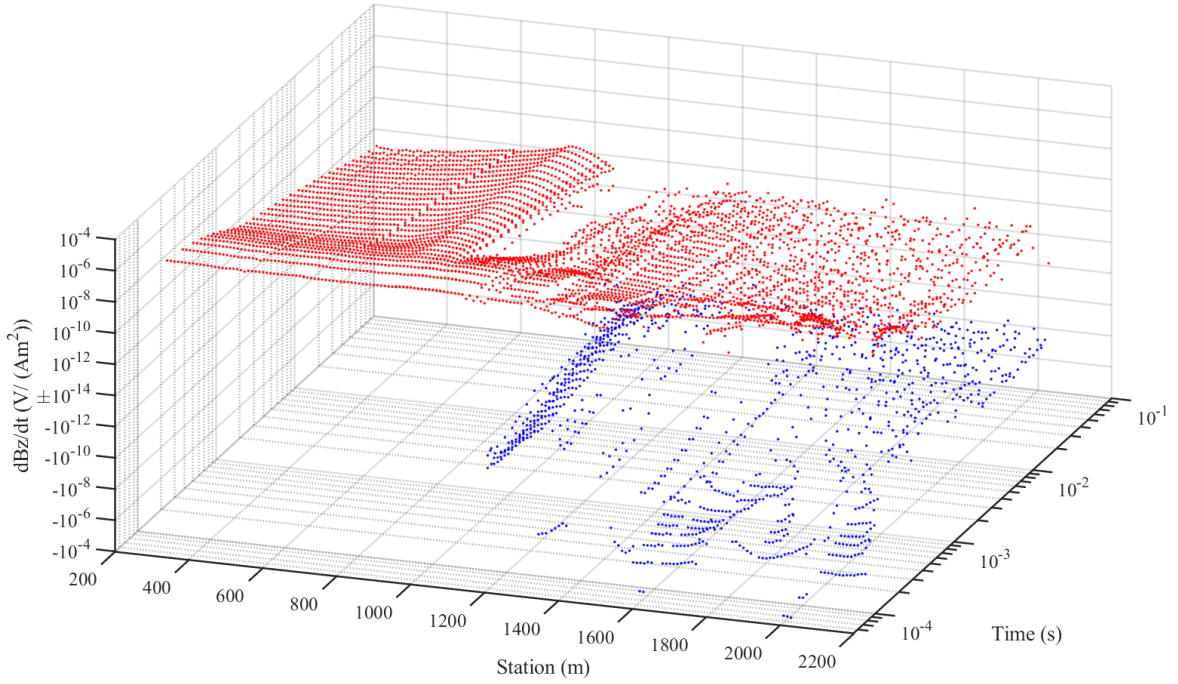

Figure 2: TEM data along the survey line. The red and blue dots indicate the positive and negative data respectively.

REFERENCES

Legault, J. M. (2015). Airborne electromagnetic systems–state of the art and future directions. *CSEG Recorder*, 40(6), 38-49.

Maurya, P. K., Foged, N., Madsen, L. M., & Christiansen, A. V. (2023). Comparison of towed electromagnetic with airborne electromagnetic and electrical resistivity tomography in a hydrogeophysical context. *Geophysical Journal International*, 235(1), 817-830.

Maurya, P. K., Grombacher, D., Lind, J., Lane, J. W., & Auken, E. (2022). Inversion of induced polarization-affected towed-transient electromagnetic data in a lateritic regolith geology: A case study from western Tanzania. Geophysics, 87(4), B247-B254.

Kang, S., & Oldenburg, D. W. (2016). On recovering distributed IP information from inductive source time domain electromagnetic data. *Geophysical Journal International*, 207(1), 174-196.

Weidelt, P. (1982). Response characteristics of coincident loop transient electromagnetic systems. *Geophysics*, 47(9), 1325-1330.

Yang, D., & Oldenburg, D. W. (2016). Survey decomposition: A scalable framework for 3D controlled-source electromagnetic inversion. *Geophysics*, 81(2), E69-E87.